

Article citation info:

Kowalik R, Kisilowski J, Łusiak T, Gil L, Stability test of Hyperloop vehicle in different movement conditions *Eksploracja i Niezawodność – Maintenance and Reliability* 2023; 25(3) <http://doi.org/10.17531/ein/169204>

Stability test of Hyperloop vehicle in different movement conditions

Indexed by:



Rafał Kowalik^{a,*}, Jerzy Kisilowski, Tomasz Łusiak^b, Leszek Gil^c

^a Polish Air Force University, Poland

^b Lublin University of Technology, Poland

^c WSEI Academy in Lublin, Poland

Highlights

- The speed and mass have the greatest influence on the stability of the Hyperloop vehicle.
- The greatest disturbance occurs between the magnets and the curved guideway.
- The method presented for determining vehicle stability eliminates the determination of the Lyapunov function.

Abstract

The guide of the Hyperloop system in the paper is mathematically represented as a continuous system along which the force from the capsule travels, with the capsule in turn represented as a discrete system. The simulations discussed in the article were used to determine the displacements of the magnet elements. ANSYS software was used to perform the simulations using finite element calculations (FEM). The stability of the capsule will be determined from the results of the displacements present in the system. Taking into account the existing conditions in the magnet and guide assembly system, the simulation results were used to analyse stability in technical and stochastic terms (Lyapunov criteria) for non-linear systems. In the technical stochastic stability analysis, the transverse displacements of the electromagnets were used. The probability of unstable Hyperloop motion was then calculated.

Keywords

stability, hyperloop vehicle, magnetic levitation

This is an open access article under the CC BY license (<https://creativecommons.org/licenses/by/4.0/>)

1. Introduction

The competence and reliability of transportation systems [41, 4] is a major logistical issue. The fifth mode of transportation, also known as vacuum rail or the Hyperloop, is a theoretical solution to multimodal transportation issues [35]. According to this idea, a vehicle—a capsule in motion carrying people travels through a tube under reduced pressure [37–39]. Due to less traffic resistance, this mode of transportation requires less infrastructure than high-speed rail and uses less energy [38]. Due to the decreased air resistance brought on by the tube's decreased pressure, there is less resistance to movement. Magnetic cushions and different running gear options have also

been employed [1].

The Hyperloop vehicle moves/floats due to an electrodynamic suspension, which suspends the rail and train in a magnetic field and uses the repelling force of the magnetic fields to propel/float the vehicle [3]. Electromagnets or a permanent magnet construction can produce the magnetic field in the train [5]. The induced magnetic field of the electric wires or the conduction belts in the tracks produce the repulsive force in the rails [2]. The voltage created in the coils and the magnetic field flux that results are too tiny at low speeds to lift the Hyperloop car off the track [6]. Thus, the Hyperloop vehicle

(*) Corresponding author.

E-mail addresses:

R. Kowalik (ORCID: 0000-0001-6431-9561) r.kowalik@law.mil.pl, J. Kisilowski (ORCID: 0000-0003-3747-0578) jkisilow@kisilowscy.waw.pl, T. Łusiak (ORCID: 0000-0003-2324-4596) t.lusiak@pollub.pl, L. Gil (ORCID: 0000-0001-8978-7388) leszek.gil@wsei.lublin.pl

must then move on its wheels, or alternatively, there must be another way to ensure that the vehicle can move on the track before it starts to hover above the track. The propulsion coils create a force between the magnets and ensure that the Hyperloop vehicle moves [7]. The coils described work in a similar way to a linear motor: current flowing through the coils creates a magnetic field along the track. The frequency of the voltage variation is synchronised with the speed of the Hyperloop vehicle (it is a type of synchronous motor). The lateral displacement caused by the magnets in the Hyperloop vehicle and the applied magnetic field cause the Hyperloop vehicle to move. Investigation of hyperloop vehicle displacement is usually limited to the vertical plane, but investigation of the lateral dynamics of the system is more important than that in the vertical plane and serves as a complement to the system in the horizontal plane [8]. It is possible to address problems with motion stability by conducting studies in the horizontal plane in the transverse direction with regard to the guideway [9].

Recently, an increasing amount of activity is considering supporting driveways at 30 meter intervals. We investigated discrete continuous systems. [10, 11] used the Runge-Kutta-Rosenbrock approach to solve the equations of motion for systems containing elastic damping elements. The authors of article [12] proposed a particular modification of his Runge-Kutta method that allows efficient integration of stiff equations. The study of the relationship between hyperloop vehicles and guideways can be considered as a cooperation between capsules and guideways [19]. Both rotational and linear motion accelerations are caused by the forces generated by the motion of the capsule. Vehicle motion, road dynamics and road bumps are all sensed by the suspension system. Tracks are usually represented in mechanical models as beams with a fixed T-shaped cross-section [23]. This guideway model is also used in the work. The displacement forces on the suspension and guideway exert forces on the guideway support [21]. These forces on the guideway beam are influenced by both the guideway reaction forces and moments of the support member [22] and the dynamic properties of the support foundation. The mathematical description of this tightly-coupled process is very complex, and appropriate assumptions must be made [20]. The vehicle under consideration can have different support

distances. A fixed support spacing value of 30 m was used in this study [24, 25]. The average speed of a Hyperloop vehicle is almost five times that of regular trains [26]. The dynamic amplification can be very significant at these extremely high speeds, which will have an immediate impact on the magnets' displacement and the safety of the vehicle's motion [31]. Additionally, the Hyperloop tube will be supported by a number of platforms that will support it vertically and permit it to move longitudinally owing to thermal expansion [33].

However, the lateral movement of the deck has not yet been examined in relation to the interaction of the Hyperloop tube with the platform [32]. In this investigation, the unbalanced loading of the train—where certain tubes are loaded but not all is what is causing the lateral vibration of the deck. Although they are outside the purview of this study, lateral loads like earthquakes and, to a lesser extent, wind, can result in lateral vibrations [34].

In a thorough and in-depth article [27], which describes the formulation of moving force and moving mass for simple spans, the problem of moving load is first mathematically defined by [32]. Vertical vehicle-bridge interaction issues have also been addressed using moving force-beam systems [8]. Parametric analysis aids analytical answers to moving load problems. To evaluate the vibration response of such systems, more intricate numerical approaches are needed because not all moving force problems can be addressed analytically [9]. For the sake of simplicity, moving load issues can be handled as static loads placed at various points throughout the structure. However, particularly for high-speed trains, the dynamic impacts of shifting loads can be significant. The peak deflection or stress induced by the dynamics of moving loads is hence characterized as DAF, or dynamic to quasi-static peak deflection [13, 14].

The paper [16] is a superb and significant monograph on moving mass loads traveling on beams. Hundreds of papers on the issue of moving loads and moving forces are described in it. Beams would still require literature citations to be added. These studies cover inertia loads, gravity loads, and permanent loads [18].

The authors, following Paracmi [29], developed more complex two-dimensional (2D) and three-dimensional (3D) models of the components of the Hyperloop system, which consisted of (3D) vehicle models that consisted of one body,

four bogies, eight bolsters, eight suspension magnets, and a magnetic force feedback controller [35]. This was done in order to investigate the impact of irregularities and resonant conditions occurring in the Hyperloop vehicle dynamics [16].

Due to its discrete-time controller, the Maglev electromagnetic train will shake while suspended. On the other hand, the HTS Maglev won't vibrate because it uses passive levitation. The existence of vibration is unavoidable, however, when the HTS Maglev vehicle is moving at high speeds [17]. The arc collision and other outside disturbances have caused some vibration in the vehicle, as was to be expected. This kind of vibration can be uncomfortable or even dangerous. The HTS Maglev system must therefore undergo dynamic testing in order to be used for rail transit in the future [30].

When studying scientific literature, it is noticeable that the number of studies that discuss the analysis of the Hyperloop vehicle as a continuous discrete system has significantly increased [15]. The response of the elastic-damping system for the Hyperloop vehicle was calculated using the Runge-Kutta-Rosenbrock algorithm [43] presents the approach for integrating the equations defining the dynamics of discrete systems.

In this study, the interaction of mass at various I-beam sites will be used to describe the interaction between the guideway and the levitation assembly of Hyperloop vehicles [48]. The magnetic levitation module's linear and angular acceleration are caused by forces that arise during the passage of the vehicle [49]. Non-linear non-uniformities appear on the guideway's surface as a result of the suspension system's reaction to accelerations in the discrete system during travel [50]. The mechanical model of the guideway is described in scientific journals as being represented by a beam with a constant cross-section resting on an elastic basis [51]. This paper also utilizes this model. The electromagnetic Hyperloop vehicle will vibrate as the suspension system moves because of the discrete model, but it won't vibrate because of the magnetic levitation phenomenon itself because there aren't any magnets in place. However, vibrations are unavoidable while the Hyperloop is traveling at a high speed [52]. The impact of the arc and other outside disturbances have generated minor vibrations in the vehicle, as is to be expected. This kind of vibration can be uncomfortable or even dangerous [44].

The tube that the Hyperloop vehicle rides on has an

underlying longitudinal structure called the guideway [45]. The ride experience and stability of the Hyperloop object are significantly impacted by the guideway's elasticity [46, 47]. The electromagnetic suspension is actively and independently regulated by the flexible guideway via a feedback controller. The electromagnetic suspension works by creating an air gap whose variation causes variation in magnetic forces. The resonance of the Hyperloop vehicle's structure causes excessive vibrations, which might result in uncomfortable ride quality or unstable suspension [3]. Therefore, a detailed analysis of the vehicle/guideway interaction is crucial for Hyperloop systems in order to guarantee stable suspension and ride quality of the Hyperloop vehicle as well as the guideway construction.

This study looks into a probabilistic scenario involving the mechanics of a Hyperloop vehicle capsule and analyses how an object would behave in a continuous, multi-span ruptured tube [40]. Using the Lagrangian approach, the equations of motion for the system in this cell were established. Simulation studies were conducted after identifying the important boundary conditions. The parameters at which the object would become static under the influence of the forces acting on the guideway were also established [42].

In this paper, the results obtained in the simulation process, mainly for the lateral movements of the electromagnet, will be used to study the stability of the motion. In the report [30], bifurcation solutions were considered as the basis for the stability study of a linear system. While such a system is theoretically possible, in practice we will study (through a simulation process) the transverse motion of electromagnets for a non-linear system with perturbations originating from the guideway [41]. These results will be used to study stochastic technical stability (a definition will be presented in the paper). This will enable the determination of the probability of unsteady motion (contact between the electromagnet and the guideway). The full procedure for this will be presented in the article. Such a process has not been investigated in any currently available work.

2. Building the physical model

Geometrical parameters, discrete models of the guideway, and the capsule are all incorporated in the mathematical equations that describe the dynamics of the Hyperloop vehicle. The

susceptibilities, together with linear and angular characteristics obtained from the coordinate systems, are also included in the mathematical description. The mathematical arguments discussed in the following paragraphs are drawn from the paper [18].

A discrete model of the Hyperloop vehicle is primed in Fig.

1. In order to represent the real object in the mechanical model under analysis, the length of the tube, denoted by L , is specified. All components comprising the Hyperloop will be treated as a discrete model (the mass m_1 is the capsule and m_2 is the lump of the levitation assembly). The individual components present in the Hyperloop vehicle model under consideration are linear susceptible components.

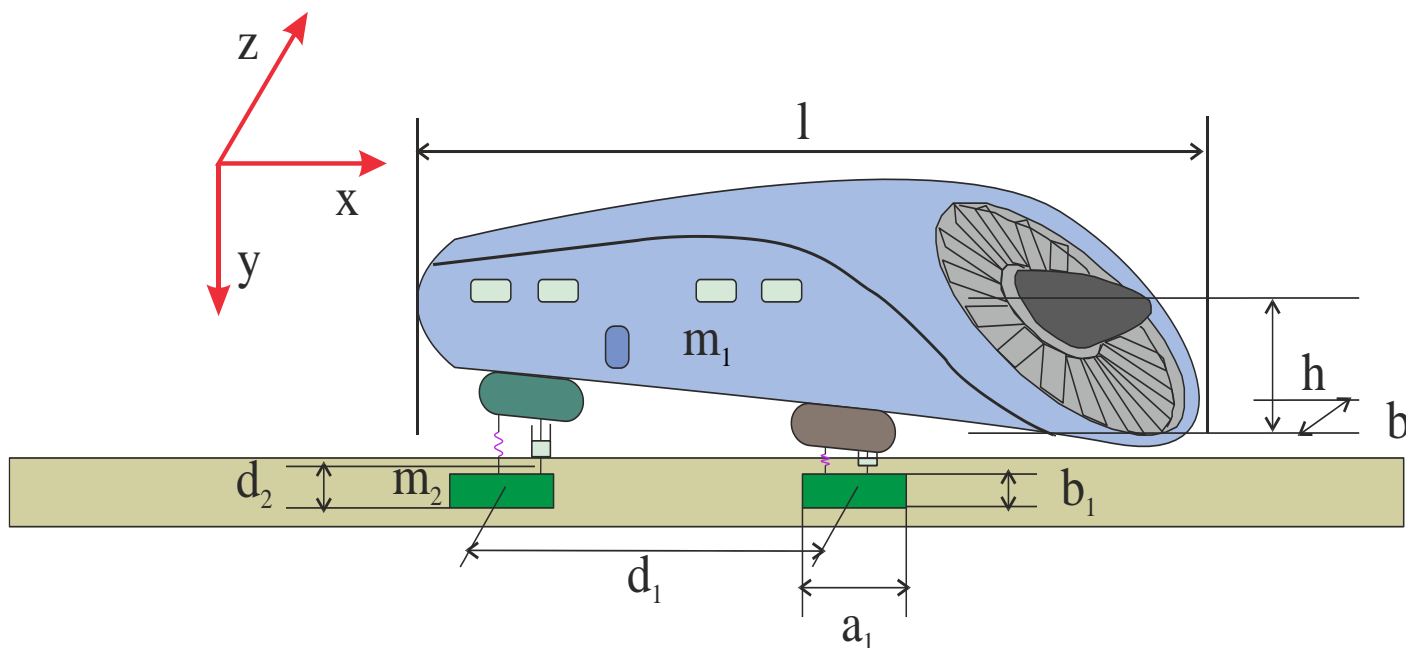


Figure 1. Capsule model discrete.

The phenomena occurring during the Hyperloop vehicle's passage and the displacements of the capsule that occur are due to the dynamics of the mass's movement along a fixed cross-section beam and are indirectly dependent on the phenomenon of magnetic levitation. In the mathematical considerations, the masses occurring in the Hyperloop vehicle are connected to each other by susceptible components. In mathematical analysis, they can be considered as a linear and non-linear component. In the mathematical derivations, it was assumed that magnitude 1 would characterise the physical phenomena occurring in the vehicle's first-stage suspension system, while phenomena occurring in the second-stage suspension system were denoted by 2. In order to determine the mathematical equations describing the displacements of the capsule and the levitation set, the quantities characterising the geometry of the Hyperloop vehicle were defined, and so by l is the length of the capsule, b is its width, while its height is determined by the parameter h . The mass objects constituting the vehicle were defined as m_1 the total mass of the capsule and m_2 the total mass

of the levitation set. The damping and elasticity coefficients present in the discrete system were defined by c_h and k_h , respectively. In order to better illustrate the clarity of the differential equations describing the dynamics of vehicle motion, two separate coordinate systems were adopted, one associated with the O1XYZ tube and the other associated with the capsule, the origin of which was assumed to be at the centre of gravity of the capsule and the levitation components. It was assumed that the axes of the coordinate system connected with the capsule and the magnetic assembly are located on the axes of symmetry of the masses of the basic elements of the vehicle. The situation is identical in the case of angular coordinates whose vectors defining velocities occurring in the system lie on the axes of the coordinate system connected with the object and characterise the dynamics of roll, yaw and inclination of the Hyperloop vehicle. In what follows, the directional cosine matrix is assumed to be zero-one (ones on the diagonal) according to the work [9].

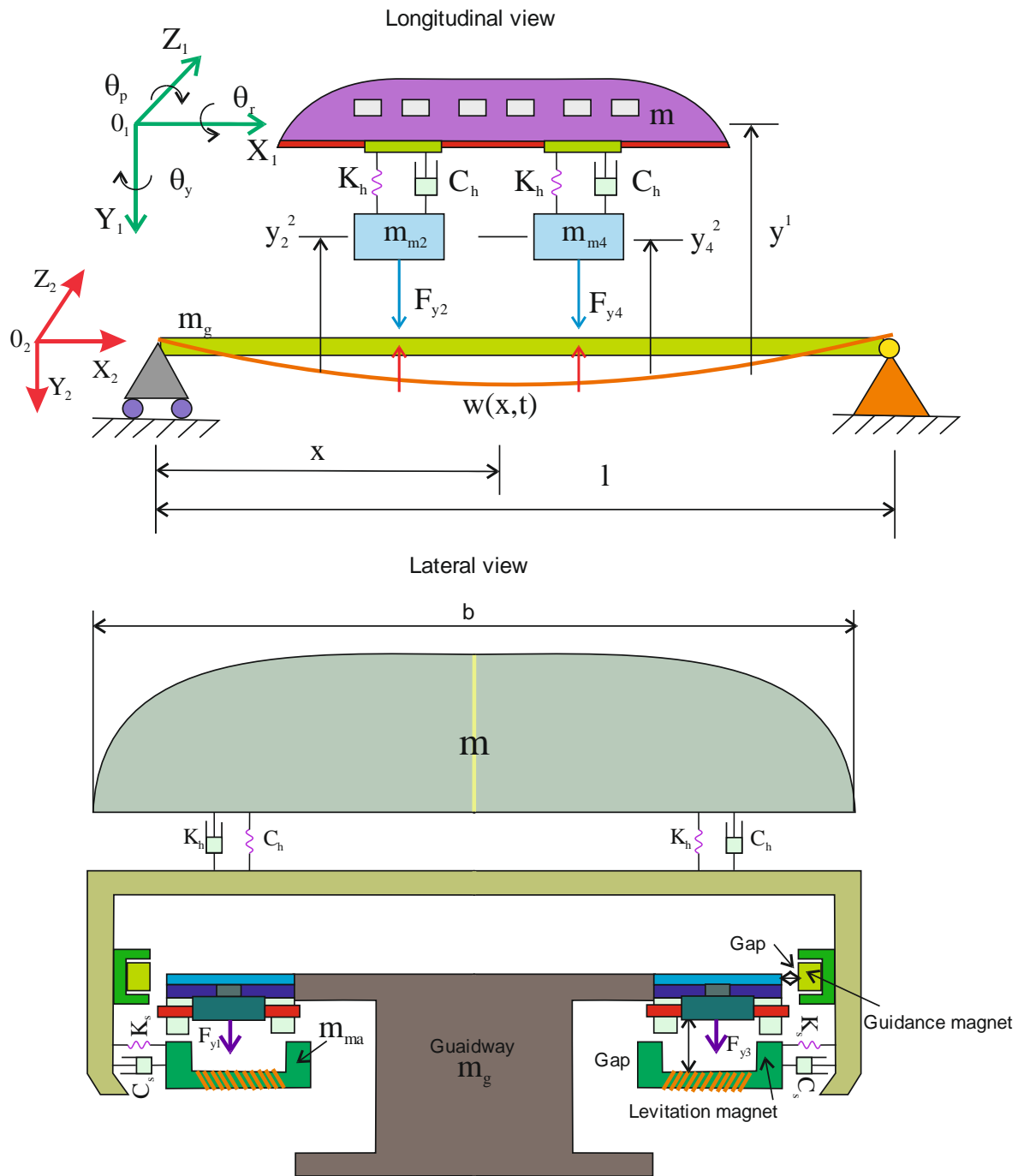


Figure 2. Hyperloop vehicle model used in the development of mathematical equations.

The suspension element in which the levitation module subassembly is contained is a closed magnetic circuit comprising magnets and a guide. As the Hyperloop object is propelled using magnetic levitation technology, the mathematical analysis must take into account the gap width occurring between the magnets and the guide and the recirculation of the components of the magnetic assembly. Which are defined by R_m and R_n ($m = 1, 2, 3$ and 4). In a further step, an attempt was made to determine the displacements $w(t,x)$ occurring on the guide, which in the model is treated as a beam

with an I-profile and a constant cross-section. An identical step was performed for the magnetic assembly whose displacements are denoted by $w_1(x, t)$.

Given the displacements of the magnetic element occurring on the set, consider all four cases defined as z_a and y_a ($a=1,2,3$ and 4 - are the number of magnets included in the levitation complex with numbers 1 and 2.). The capsule y - and z -axis displacements occurring in the first and second Hyperloop suspension components can be calculated using the assumptions made. The subsequent equations were obtained for the magnetic

force and linear elastic-damping components that appeared in the generated discrete model: the spring pressure needed to move a capsule inside a tube:

Spring forces:

$$K_h(y_1 - y_{a2}), K_s(z_1 - z_{a2}), (a = 1, 2, 3, 4) \quad (1)$$

damping forces acting on the capsules:

$$C_h \left(\frac{dy_1}{dt} - \frac{dy_{a2}}{dt} \right), C_h \left(\frac{dz_1}{dt} - \frac{dz_{a2}}{dt} \right), (a = 1, 2, 3, 4) \quad (2)$$

Magnetic force of magnetic levitation system:

$$F_{ya} = \frac{\varphi_{a1}(t)}{\mu_0 A_a}, F_{za} = \frac{\varphi_{a1}(t)}{\pi} \cdot \frac{a_2 z_{a2}}{\mu_0 A_{a1}}, a = (1, 2, 3, 4) \quad (3)$$

where, in equation (3), F_{ya} and F_{za} denote the magnetic force components appearing during transverse and vertical motion, with μ_0 denoting the magnetic permeability in vacuum, $A_a = a_{2a} \times (b_{2a} - z_{2a}), a = (1, 2, 3, 4)$

In the phenomenon of magnetic levitation, the magnetic field generated in this area is defined in the mathematical equations by the magnitude ϕ_a and is closely related to the resistance of the passive elements that make up the magnetic module and are defined by R_a . The mathematical relationship is as follows:

$$\phi_a = \frac{N I_a(t)}{R_a}, a = (1, 2, 3, 4) \quad (4)$$

The quantity N appearing in the equation denotes the number of turns occurring in the eclectic circuit and by the parameter I_a the current occurring in the circuit is specified.

$$R_a = R_0 + r s_a(t), a = (1, 2, 3, 4) \quad (5)$$

where $r = 2/\mu_0 A_0$, $s_a(t) = \delta_a(t) - \delta_0$ produces a disturbance in the y-axis, but the reluctance or gap parameter R_0 between the magnet assembly and the guide at rest is equilibrium. The air gap is determined by the amount δ_a , which is defined by the relationship:

$$\delta_a(t) = y_{a2}(t) - w_a(t), a = (1, 2, 3, 4) \quad (6)$$

3. Motion equations for Hyperloops

To determine the equations of motion of the Hyperloop vehicle, d'Alembert's principle was used, resulting in:

$$\begin{aligned} m_v \frac{d^2 y_{a2}}{dt^2} - C_h \left(\frac{dy_1}{dt} - \frac{dy_{a2}}{dt} \right) - K_h(y_1 - y_{a2}) &= \\ m_g - F_{ya}, a = (1, 2, 3, 4) & \\ \\ m_v \frac{d^2 z_{a2}}{dt^2} - C_h \left(\frac{dz_1}{dt} - \frac{dz_{a2}}{dt} \right) - K_s(z_1 - z_{a2}) &= \\ F_{za}, a = (1, 2, 3, 4) & \end{aligned} \quad (7)$$

$$\begin{aligned} m_g \frac{d^2 y_1}{dt^2} + C_h \sum_{a=1}^4 \left(\frac{dy_1}{dt} - \frac{dy_{a2}}{dt} \right) + \sum_{a=1}^4 K_h(y_1 & \\ - y_{a2}) &= m_g g \end{aligned}$$

$$m_g \frac{d^2 z_1}{dt^2} + C_s \sum_{a=1}^4 \left(\frac{dz_1}{dt} - \frac{dz_{a2}}{dt} \right) + \sum_{a=1}^4 K_s(z_1 - z_{a2}) = 0$$

and

$$\begin{aligned} J_p \frac{d^2 \theta_p}{dt^2} + C_p \frac{d^2 \theta_p}{dt^2} - K_p \theta_p & \\ &= (J_r - J_y) \frac{\theta_r}{dt} \cdot \frac{\theta_y}{dt} - L_p \\ J_y \frac{d^2 \theta_y}{dt^2} + C_y \frac{d^2 \theta_y}{dt^2} - K_y \theta_y & \\ &= (J_p - J_r) \frac{\theta_p}{dt} \cdot \frac{\theta_r}{dt} - L_y \\ J_r \frac{d^2 \theta_r}{dt^2} + C_r \frac{d^2 \theta_r}{dt^2} - K_r \theta_r & \\ &= (J_y - J_p) \frac{\theta_y}{dt} \cdot \frac{\theta_p}{dt} - L_r \end{aligned} \quad (8)$$

The quantities included in equation (8) are $\theta_p, \theta_y, \theta_r$ angles of rotation in the $O_1 X_1 Z_1 Y_1$ coordinate system associated with the capsule in the roll, yaw and pitch directions. The moment of inertia occurring in the system, defined by J_p, J_y, J_r was defined in the lower order.

The moment of inertia value for the second suspension stage of a hyperloop vehicle is written as:

$$\begin{aligned} J_p &= \frac{1}{12} m_v [L^2 + h^2] \\ J_y &= \frac{1}{12} m_v [L^2 + b^2] \\ J_r &= \frac{1}{12} m_v [h^2 + b^2] \end{aligned} \quad (9)$$

The parameters L_p, L_y, L_r visible in the equation above are the inertial forces. The mathematical notation is as follows:

$$\begin{aligned} L_p &= \frac{d_1}{2} \left[C_h \left(\frac{dy_{4,2}}{dt} + \frac{dy_{3,2}}{dt} - \frac{dy_{2,2}}{dt} - \frac{dy_{1,2}}{dt} \right) \right. \\ &\quad \left. - K_h(y_{a,2} + y_{a,2} - y_{a,2} - y_{a,2}) \right] \cos \theta_p, a = (1, 2, 3, 4) \\ L_y &= \frac{d_1}{2} \left[C_s \left(\frac{dy_{a,2}}{dt} + \frac{dy_{a,2}}{dt} - \frac{dy_{a,2}}{dt} - \frac{dy_{a,2}}{dt} \right) \right. \\ &\quad \left. - K_s(y_{a,2} + y_{a,2} - y_{a,2} - y_{a,2}) \right] \cos \theta_y, a = (1, 2, 3, 4) \\ L_r &= \frac{d_2}{2} \left[C_h \left(\frac{dy_{a,2}}{dt} + \frac{dy_{a,2}}{dt} - \frac{dy_{a,2}}{dt} - \frac{dy_{a,2}}{dt} \right) \right. \\ &\quad \left. - K_h(y_{a,2} + y_{a,2} - y_{a,2} - y_{a,2}) \right] \cos \theta_r, a = (1, 2, 3, 4) \end{aligned} \quad (10)$$

The displacement caused by the guideway can be expressed by the following formula:

$$\begin{aligned}
EJ \frac{\partial^4 w}{\partial x^4} + C_h \frac{\partial w}{\partial t} + \rho \frac{\partial^2 w}{\partial t^2} \\
= \eta_1(t, x) \sum_{a=1}^2 \frac{F_{ya}}{L_{a2}} \\
+ \eta_2(t, x) \sum_{a=1}^4 \frac{F_{ya}}{L_{a1}}
\end{aligned} \quad (11)$$

in which

$$\begin{aligned}
\eta_1(t, x) &= \begin{cases} 1 & \text{for } vt - \frac{La_1}{2} \leq x \leq vt + \frac{La_1}{2} \\ 0 & \text{otherwise} \end{cases} \\
\eta_2(t, x) &= \begin{cases} 1 & \text{for } vt - d_1 - \frac{La_2}{2} \leq x \leq vt - d_1 + \frac{La_2}{2} \\ 0 & \text{otherwise} \end{cases}
\end{aligned} \quad (12)$$

where $La_1 = La_2$ and are the respective electromagnetic forces generated by the first and second levitation sets.

4. Discrete model of a Hyperloop vehicle

The levitation system of the Hyperloop facility in question uses an articulated trolley system. The trolley on which the levitation

module is mounted has four magnetic systems on each side, and these are magnetised with different polarities alternately. On the other side, the levitation coils are on a slide and connected to others on the opposite side of the slide. When the capsule moves and there is a change in the magnetic field in front of these levitating coils, an induced current flows in these coils and an electromagnetic force is generated. As a result, having these parameters in hand, it is possible to write an equally motion for the Hyperloop vehicle:

$$m_v \frac{d^2 y_2}{dt^2} + C_h \left(\frac{dy_2}{dt} - \frac{dy_1}{dt} \right) + K_h (y_2 - y_1) = 0 \quad (13)$$

The formula uses the following designation for the mass of the capsule m_v , the displacements formed in the vertical direction of the capsule are denoted by y_2 and the vertical displacements of the levitation system are denoted by y_1 . The damping occurring in the second-stage suspension system under consideration is defined by C_h and the stiffness on this suspension is K_h .

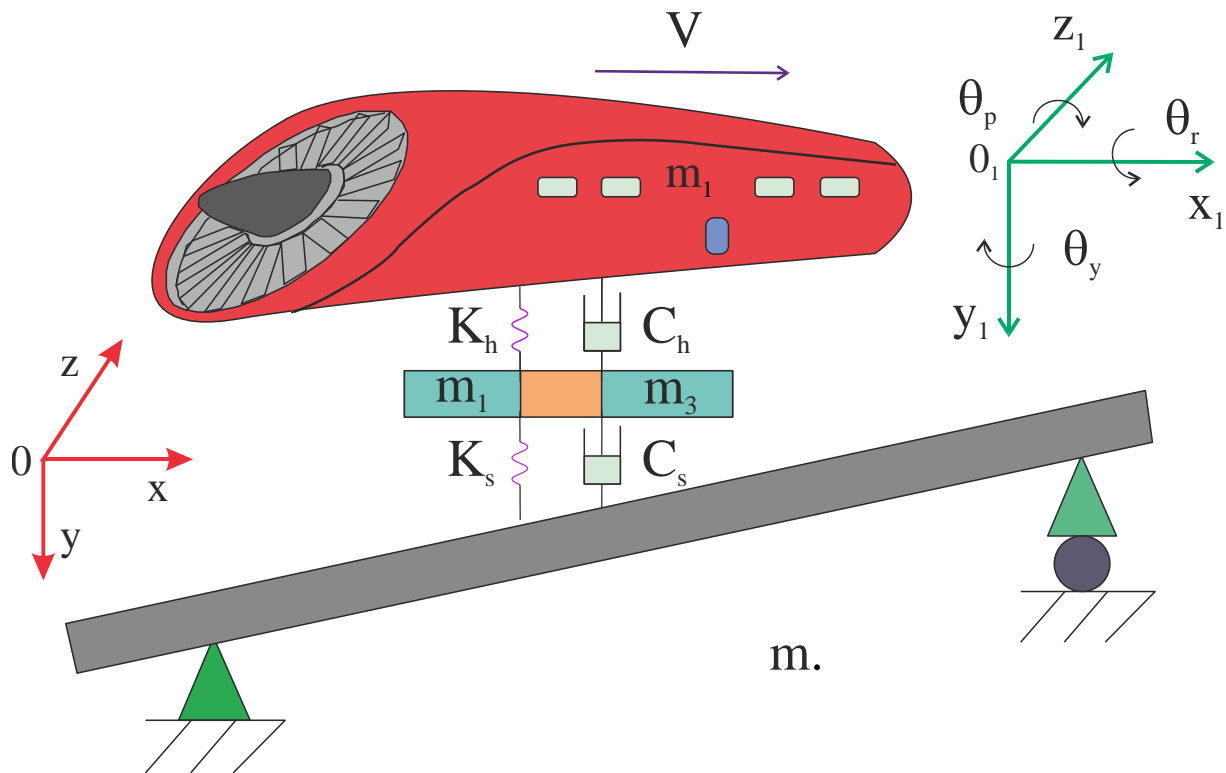


Figure 3. Horizontal movement of the Hyperloop vehicle.

The mathematical notation of the dynamics of movement in the vertical direction for the suspension of the levitating module is defined as:

$$\begin{aligned}
m_v \frac{d^2 y_1}{dt^2} - C_h \left(\frac{dy_2}{dt} - \frac{dy_1}{dt} \right) - K_h (y_2 - y_1) \\
+ C_s \left(\frac{dy_1}{dt} - \frac{dw(x, t)}{dt} \right) \\
+ K_s (y_1 - w(x, t)) = 0
\end{aligned} \quad (14)$$

In formula (14), the individual quantities represent successively in $w(x, t)$ the vertical displacement of the guide at

time t and place x , the mass of the levitating set - m_1 , the

damping occurring in the first suspension stage - C_s and the stiffness in this system is K_s .

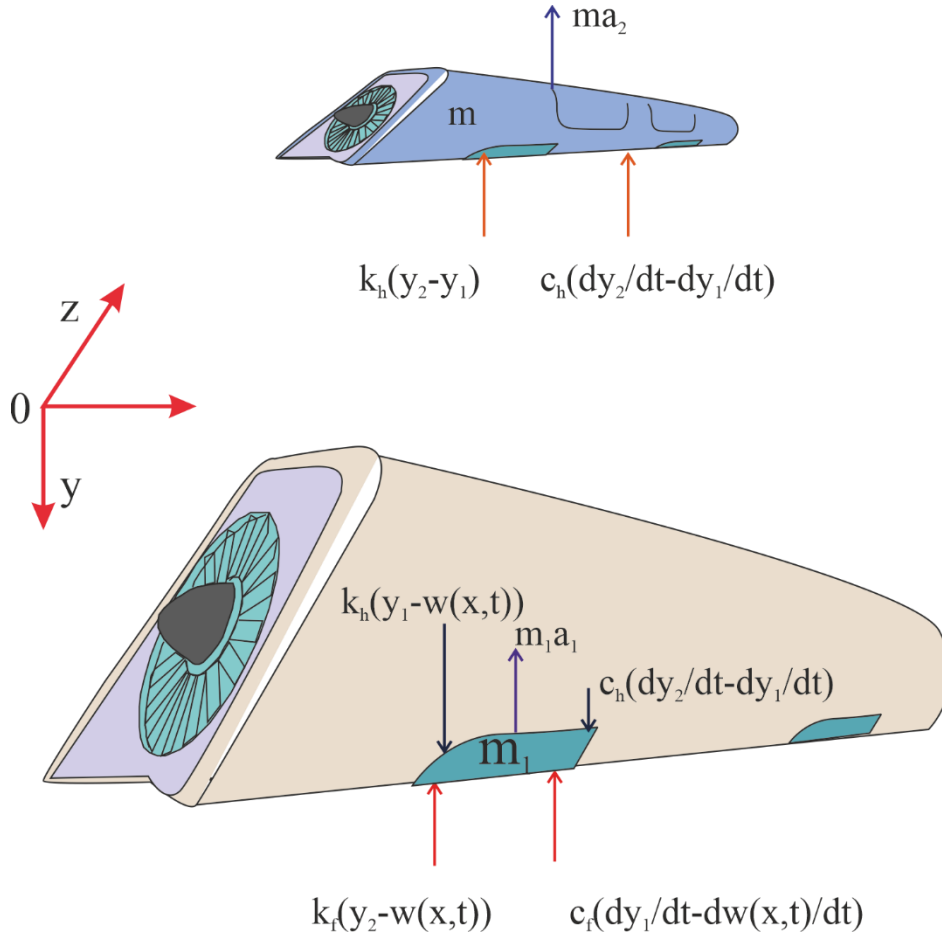


Figure 4. Location of the main coordinate system complete for the Hyperloop vehicle.

The natural vibrations occurring in the system under consideration are expressed by the equation:

$$\begin{aligned} \frac{d^2 A_k(t)}{dt^2} + 2\zeta_k \omega_k \frac{dA_k(t)}{dt} + \omega_k^2 A_k(t) &= (m_m + m_v)g \\ + c_s \left(\frac{dy_1}{dt} - \frac{dw(x,t)}{dt} \right) &+ k_s(y_1 \\ - w(x,t)) \frac{\sqrt{2}}{m_v L} \sin\left(\frac{k\pi vt}{L}\right) &= 0 \end{aligned} \quad (15)$$

where ζ_k is the irregularity appearing on the guideways.

In a further mathematical consideration, the equation for the value of the movement occurring on the guide can be determined:

$$\begin{aligned} w(x,t) &= \sum_{k=1}^{\infty} A_k(t) \phi_k(x) \\ &= \sum_{k=1}^{\infty} A_k(t) \sqrt{2} \sin\left(\frac{k\pi vt}{L}\right) \end{aligned} \quad (16)$$

$A_k(t)$ – the course of the displacements generated on the

guideway.

5. Stochastic technical stability (STS)

The STS definition was taken from the book [3]. Stability in the Lyapunov sense is determined by STS. After giving the definition, we'll discuss how this stability relates to Hyperloop motion. One of the most crucial aspects of studying the dynamics of mechanical, electromechanical, and electrical systems is the stability of dynamic processes in the Lyapunov sense. Let's outline the STS.

Take the differential equation as an example:

$$\begin{aligned} \frac{d\bar{x}}{dt} &= f(\bar{x}, t, \bar{\xi}(t, v)) \\ \bar{x}(0) &= \bar{x}_0 \end{aligned} \quad (17)$$

where:

$$\begin{aligned} \bar{x} &= [x_1, x_2, \dots, x_n]^T, \\ \bar{f} &= [f_1, f_2, \dots, f_n]^T, \\ \bar{\xi} &= [\xi_1, \xi_2, \dots, \xi_n]^T, \end{aligned}$$

where $x = (x_1, \dots, x_n)$ and $f(x, t, y) = (f_1, \dots, f_n)$ are vectors,

while $\xi(t) = (\xi_1, \dots, \xi_n)$, $t \geq 0$ is a stochastic process that describes a randomly occurring disturbance. For the function $f(x, t, y)$ assumptions have been made that it is specified for each $x \in E_n, y \in E_n$ and $t \geq 0$. It was also assumed that for the stochastic process $f(0, t, \xi(t))$ occurs

$$P\left\{\int_0^T |f(0, t, \xi(t))| dt < \infty\right\} = 1, \text{ for each } T > 0, \quad (18)$$

and that there exists a stochastic process $f(X, t, \xi(t))$ satisfying the Lipschitz criterion in the interval $[0, T]$

$$|f(\bar{x}', t, \bar{\xi}(t, v)) - f(\bar{x}, t, \bar{\xi}(t, v))| \leq \eta(t, v) |\bar{x}' - \bar{x}| \quad (19)$$

for another process $\eta(t)$, absolutely integrable in the given interval. This presumption is comparable to the function continuity criteria.

The definition of technical stochastic stability is: if every solution of equation (17), whose initial conditions (t, t_0, x_0) are contained in the area ω , belongs to the area Ω with probability $1 - \varepsilon$, then the system (17) is technically stochastically stable with respect to ω, Ω and the process $\xi(t)$ with probability $1 - \varepsilon$ (Fig.5).

$$P\{\bar{x}(t, t_0, \bar{x}_0) \in \Omega\} > 1 - \varepsilon \text{ into } x_0 \in \omega \quad (20)$$

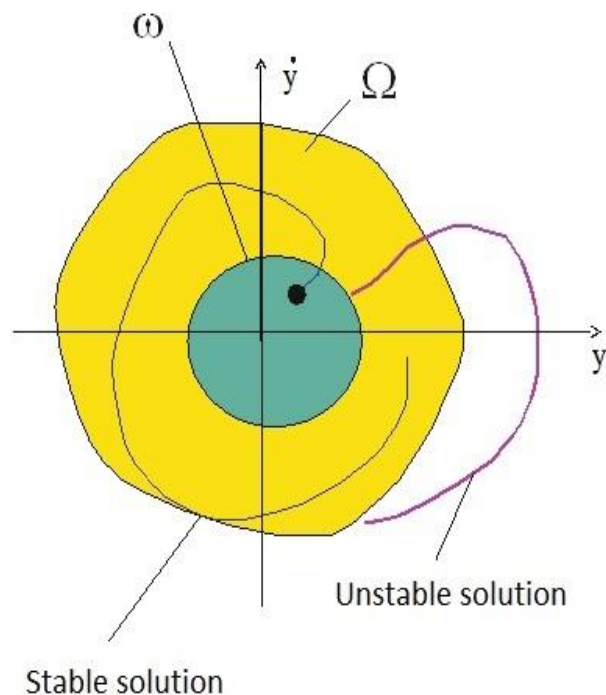


Figure 5. Graphical interpretation of the stochastic technical stability.

We provide the traditional concept of Lyapunov stability here as a reminder [3]. The Lyapunov definition is one of the

original and fundamental definitions of mechanical system stability. n first-order differential equations of the form represent the motion of a mechanical system in its description.

$$\frac{dx}{dt} = f(t, x) \quad (21)$$

where by $f(t, x) = F(t, \zeta + x) - F(t, \zeta)$, where ζ stands for undisturbed movement, while x - disturbance occurring [28].

The solution $\xi = \xi(t)$ of the system described by equation (21) is Lagrangian stable for $t \rightarrow \infty$ if for any $\varepsilon > 0$ and $t_0 \in (a, \infty)$ there exists $\eta(\varepsilon, t_0) > 0$ such that:

- all solutions (trajectories) $x = x(t)$ of equations (21), including $\xi(t)$ satisfy the condition

$$\|x(t_0) - \xi(t_0)\| < \eta \quad (22)$$

and are defined in the future, i.e. in the interval $[t_0, \infty)$;

- for these solutions, the inequality occurs

$$\|x(t) - \xi(t)\| < \varepsilon \text{ into } t \in [t_0, \infty). \quad (23)$$

The verbal interpretation of this notation after [17] is that the trajectory $\xi(t)$ of equations (21) is stable when the perturbed solution $x(t)$ is located in a narrow region ε around $\xi(t)$ (Fig. 6). This means that the region ε is the limit within which the perturbed solution can be found, so that the stability of the analysed system can be established. Failure to determine the probability of the perturbed solution being close to the correct solution makes it impossible to subject the system to random perturbations and analyse their effect on the motion of that system.

In the study of stability in the Lyapunov sense, there are limitations on the extensibility of the solution of equation (21) to infinity, and the conclusion of this solution for the area defined by the parameter $\varepsilon > 0$.

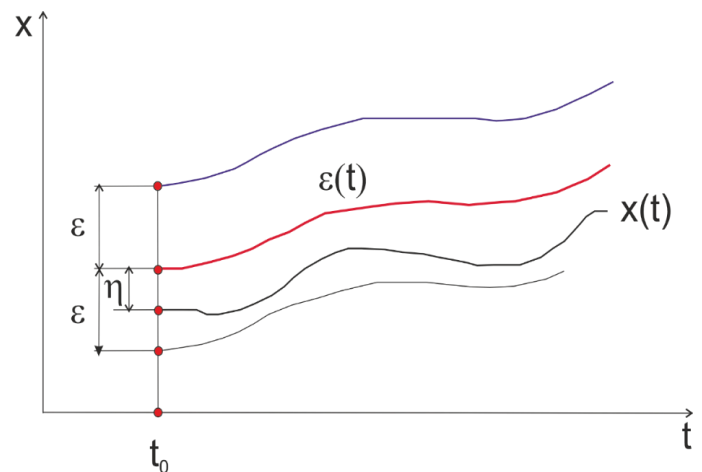


Figure 6. Lyapunov-style stability graphically interpreted [28].

Testing stability according to the classical definition of Lyapunov requires the determination of the Lyapunov function, most often denoted by V in mechanics. Unfortunately, there are currently no rules that allow the determination of this function. Most often the determination of this function requires it to be "guessed".

In the STS study, no such procedure is required. What is required is to define the area Ω and to find a solution describing the dynamics for a given generalised coordinate. For the Hyperloop, we assume that the positive extent of the area Ω is the clearance, which is described by relation (6) and in Fig.2 the distance between the guide and guidance magnet. The second gap, which appears in Fig.2, may have larger magnitudes, as the size of this gap also depends on the deflection of the susceptible elements. This gap can be taken up in different magnitudes. In our simulation studies, a gap size of 8 mm was adopted. The magnitude of the gap variation is the transverse motion of the electromagnet - in the model the y_1 coordinate from equation (7). As a result of the simulation, this motion is a random variable, i.e. a stochastic signal (the set of determinants is time), whose analysis will be conducted on the basis of a single realisation. In order for such an analysis to be carried out, it must be investigated or assumed whether the stochastic signal has the properties of stationarity of order two and global ergodicity. In our study, we have made such an assumption, which allowed the analysis on the basis of a single realisation. We will then determine a histogram of the changing magnitudes of the electromagnetic motion in the y -direction for a guide magnet. We assume a significance level of $\alpha = 0,05$ for further testing. Then, using the Kolmogorov-Smirnov test, we determine the form of the function describing the probability of a given magnitude of slack. With such a function, it is possible to determine the probability of movement of electromagnets with a magnitude of 8 mm, i.e. there will be contact between the guiding electromagnet and the guide. This is the magnitude in which the movement is unstable. As shown graphically in Figure 5, such a probability can be determined from the relationship:

$$P(y_1) = \int_{-\infty}^{y_1=8\text{ mm}} \delta(y) dy \quad (24)$$

Guide inequalities have been omitted from the considerations, due to their very small magnitudes. Probabilities will be determined for different Hyperloop movement

conditions. The procedure prepared in this way will be carried out obtaining results in the simulation process.

6. Simulation study

The following quantities characterising the Hyperloop vehicle were assumed in the simulation [36]:

Table 1. Geometrical and mechanical parameters used in the simulations for the Hyperloop vehicle.

Hyperloop vehicle parameters		
Total Secondary Damping	c_z	8.46×10^4 [Ns/m]
Length of vehicle	L	25 [m]
Primary Total Damping	C_h	2.15×10^6 [Ns/m]
Mass Levitation frames	m_m	22000 [kg]
Carriage body pitch inertia	I_v	1.75×10^6 [kgm ²]
Carriage mass	m_v	15000 [kg]
Primary Total Stiffness	K_h	1.18×10^8 [N/m]
Secondary Total Stiffness	K_z	6.812×10^5 [N/m]

The simulation process adopted the guide model shown in Figure 7.

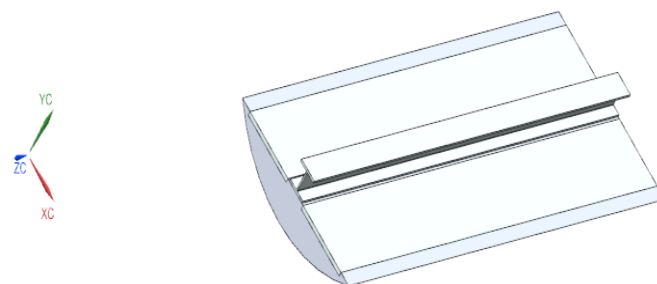


Figure 7. CAD model of a guideway of Hyperloop objects [18]

The simulations resulted in the movements of four magnets, for speeds of 1,000 km/h and 2,000 km/h. Simulations were carried out for two cases: movement of the capsule in a straight tube and movement of the capsule along a curved tube with a radius of 200,000 m. Results for the transverse motion of the electromagnets were recorded. The primary stability criterion was the size of the gap between the guide magnet and the guide. An example of the transverse displacement result for 4 electromagnets for a speed of 1000 km/h along a straight tube is shown in Fig. 8. Fig. 9 shows the transverse displacement for 4 electromagnets for a speed of 1000 km/h along a curved tube. Figures 10 and 11 show the transverse displacement for 4 electromagnets for a speed of 2000 km/h along a straight and curved tube.

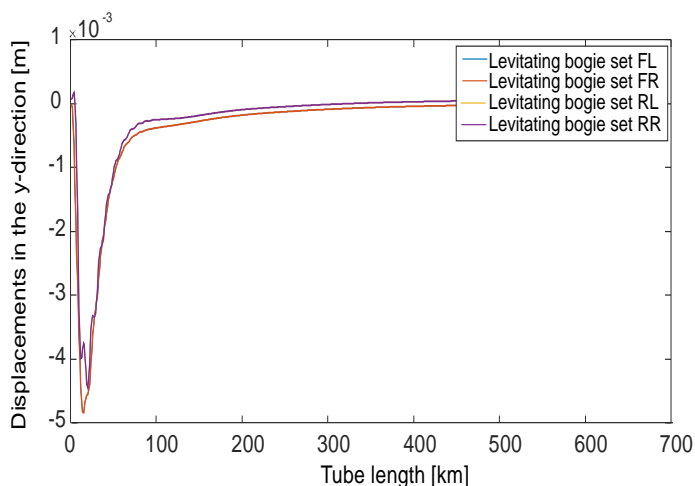


Figure 8. Displacement of the levitation set at 1000 km/h in a straight tube.

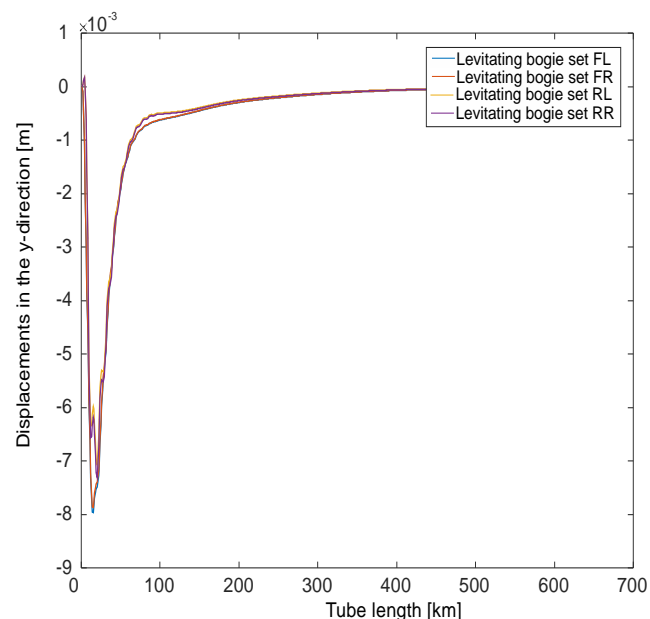


Figure 11. Displacement of levitation set at 2000 km/h in a curved tube with radius $R= 200\,000$ metres.

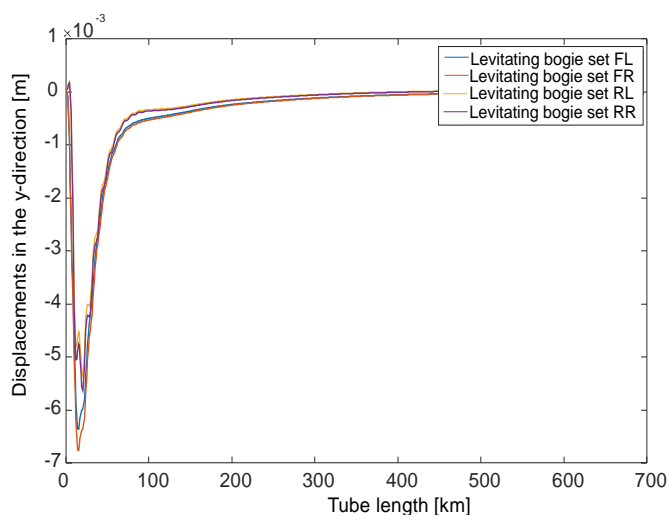


Figure 9. Displacement of levitation set at 1000 km/h in a curved tube with radius $R= 200\,000$ metres.

In Figure 8, orange is for levitation magnet movement and purple is for guidance magnet movement. In Figure 9, the maximum displacement is for the levitation magnet movement. The purple colour indicates guidance magnet motion. The results show that for a speed of 1000 km/h, only the maximum displacement values change for both the levitation magnet and guidance magnet movements. For a speed of 2000 km/h, the maximum displacement magnitudes for both the straight and curved tube show levitation magnet movements. For guidance magnet movements, the maximum magnitudes of the lateral displacements do not exceed 8 mm.

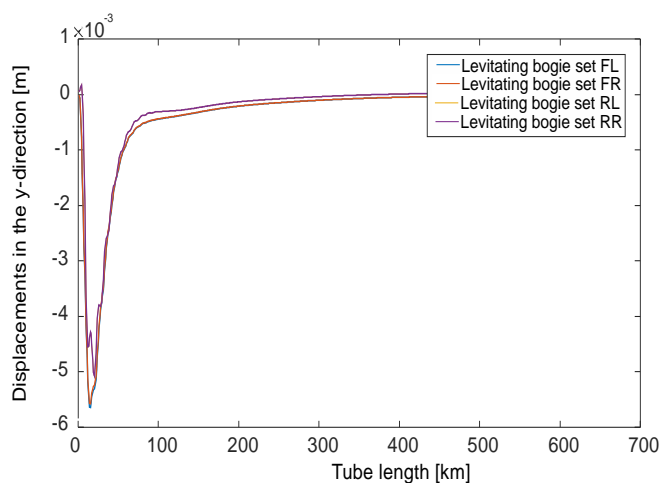


Figure 10. Displacement of the levitation set at 000 km/h in a straight tube.

Simulations for different radii of curvature of the tube were also investigated. For radii smaller than 200,000 m, there was a process of contact between the guidance magnet and the guide, leading to destruction of the systems. Only at a radius of 200,000 m was possible movement recorded. With the graphs in hand, histograms were determined and a probability distribution was selected in the form of a normal curve at a significance level of $\alpha=0.05$. These curves characterise the mean values and standard deviations. For these distributions, the probability of steady state movement was determined. A set of these results are summarised in Table 2.

Table 2. Summary of simulation results for stability testing for 1000 km/h, where FL - first levitation set with magnets located on the left side, FR - first levitation set with magnets located on the right side, RL - second levitation set with magnets located on the left side, RR - first levitation set with magnets located on the right side.

Parameters of normal distribution (Kolmogorov-Smirnov test for one sample)	Mean value	Standard deviation	Probability of steady motion
Speed 1000 km/h straight tube			
Displacements of the levitation set in the y-direction for FL magnets	0.000643564	0.001500849	0.9999/0.00356
Displacements of the levitation set in the y-direction for FR magnets	0.00064351028	0.001500660	0.9999/0.00426
Displacements of the levitation set in the y-direction for RL magnets	0.0005307696	0.00125932818	0.9999/0.00356
Displacements of the levitation set in the y-direction for RR magnets	0.000530715685	0.0012591756	0.9999/0.00357
Speed 1000 km/h curved tube with a radius of 200,000 metres			
Displacements of the levitation set in the y-direction for FL magnets	0.00135772256	0.0041107885	0.99024/0.01077
Displacements of the levitation set in the y-direction for FR magnets	0.00135765939	0.00411063733	0.99024/0.01077
Displacements of the levitation set in the y-direction for RL magnets	0.00124279509	0.003959562	0.98862/0.01125
Displacements of the levitation set in the y-direction for RR magnets	0.0012427319	0.0039426835	0.99024/0.01077

Table 3. Summary of simulation results for stability testing for 1000 km/h

Parameters of normal distribution (Kolmogorov-Smirnov test for one sample)	Mean value	Standard deviation	Probability
Speed 2000 km/h straight tube			
Displacements of the levitation set in the y-direction for FL magnets	0.0053174648	0.01086606	0.88982/0.03149
Displacements of the levitation set in the y-direction for FR magnets	0.0053159854	0.01086289500	0.9039/0.03148
Displacements of the levitation set in the y-direction for RL magnets	0.00469238594	0.0097347381	0.9385/0.02814
Displacements of the levitation set in the y-direction for RR magnets	0.00469120652	0.00973194839	0.9039/0.02813
Speed 2000 km/h curved tube with a radius of 200,000 metres			
Displacements of the levitation set in the y-direction for FL magnets	0.006915739420	0.016245364	0.81912/0.04595
Displacements of the levitation set in the y-direction for FR magnets	0.00681447120	0.0162416190	0.81915/0.04594
Displacements of the levitation set in the y-direction for RL magnets	0.00618407671	0.01514287177	0.82554/0.04266
Displacements of the levitation set in the y-direction for RR magnets	0.00618280847	0.01513931248	0.82557/0.04265

The measurements were then repeated for the same levitation trolley parameters, but at a speed of 2000 km/h. The results obtained from this analysis are presented in Table 3.

Two probability quantities are given in Table 2 and Table 3: the first quantity represents the probability of steady state motion and the second quantity represents the probability of unsteady motion. In Table 1, RL and RR are the guide magnet and FL and FR are the levitation magnet. From a stability point

of view, according to the earlier definition, Ω is assumed to refer to the clearance between the guide magnet and the guide.

The obtained results of the transverse displacements of the guiding and levitation magnets made it possible to determine the probability of the occurrence of a steady state motion, i.e. one whose solution falls within the boundary Ω , Fig.5. Such a study gives an answer as to what is the probability of the movement of the magnets (guiding and levitation) occurring.

According to Figure 5, if the trajectory of the solution coincides with the boundary Ω , which in our case means the clearance between the guide and the magnets, then with a certain probability (which is given in Table 1 as the second value, for the displacement of the levitation set in the y-direction for the FL magnets it is 0.00356) non-static motion occurs. Such tests were carried out for speeds of 1000 km/h and 2000 km/h along a guideway - straight tube and a guideway - curved tube with a radius of 200000 m. As can be seen from the results presented, the probability of unsteady motion is at least ten times higher for motion along a guide-tube-curved tube. The guide-tube FL probability of unsteady motion is 0.00356, and for motion in a curved tube the probability of unsteady motion is 0.01077. Both values were determined for a speed of 1000 km/h. For a speed of 2000 km/h, the occurrence of unsteady motion is in a similar relationship.

7. Conclusions

This paper demonstrates the possibility of using stochastic technical stability to test Hyperloop stability - in the Lyapunov sense. So far, stability testing has been performed for linear stability without disturbances. This method makes it possible to study the stability of linear and non-linear systems with arbitrary external disturbances by determining the possible

ranges of motion of solids relative to each other, i.e. the size of the gap which in stability is defined as Ω . Such tests can be carried out for various conditions of motion: change of velocity, change of tube position, change of tube support point spacing, change of the mathematical description of the guide (an Euler-Bernoulli beam is assumed in the tests). This type of stability study is impossible for different types of mathematical descriptions of stability, as it usually leads to the determination of the Lyapunov function (which cannot be defined and must be guessed at). This type of stability test eliminates this type of inconvenience.

The paper investigates what size of radius of curvature and tube allows for steady and unsteady motion between the magnet and guide. The study determined such a radius, which was 200,000 m, for which the technical stochastic stability of the movement of the magnets relative to the guide was tested. The proposed method makes it possible to study stability for different radii of curvature of the tube and different magnitudes of external disturbances. The proposed model also makes it possible to study the accelerations on the curve, which consist of three components - centripetal acceleration, Coriolis acceleration and lift acceleration. These can be determined using simulation methods.

References

1. Abdelrahman, A.S., Sayeed, J., Youssef, M.Z., Hyperloop Transportation System: Analysis, Design, Control, and Implementation, IEEE Trans. Ind. Electron., 2017, 65, 7427–7436. <https://doi.org/10.1109/TIE.2017.2777412>
2. Blatnický M., Dizo J., Drozdziel P., FEM analysis of main parts of a manipulator for mounting a compressor to a car equipped with a pneumatic suspension system, Diagnostyka, vol.21, no. 2, pp. 87-94, 2020. DOI 10.29354/diag/122549
3. Bogusz W., Technical stability, Warsaw: IPPT PAN, 1972.
4. Borucka A. Three-state Markov model of using transport means, 18th International Scientific Conference on Business Logistics in Modern Management, 2018, 18, 3-19
5. Braun, J.; Sousa, J.; Pekardan, C., Aerodynamic design and analysis of the Hyperloop, AIAA J. 2017, 55, 4053–4060. <https://doi.org/10.2514/1.J055634>
6. Chaidez E., Bhattacharyya S. P. and Karpets A. N., Levitation Methods for Use in the Hyperloop High-Speed Transportation System, Energies 2019, 12(21), 4190, <https://doi.org/10.3390/en12214190>
7. Chen X., Ma W. and Luo S., "Study on stability and bifurcation of electromagnet-track beam coupling system for EMS maglev vehicle," *Nonlinear Dynamics*, vol. 101, pp. 2181-2193, 2020. <https://doi.org/10.1007/s11071-020-05917-8>
8. Chen X., Ma W., Luo S. and Zou R., "A vehicle-track beam matching index on EMS Maglev transportation system," *Arch. Appl. Mech.*, 2019. <https://doi.org/10.1007/s00419-019-01638-6>
9. Dodson B., "Beyond the hype of Hyperloop: An analysis of Elon Musk's proposed transit system," 22nd August 2013. [Online]. Available: <https://newatlas.com/hyperloopmusk-analysis/28672/>.
10. Gutowski R., Podstawy teorii stateczności ruchu układów dyskretnych i ciągłych, Politechnika Warszawska, Wydział Mechaniczny

Energetyki i Lotnictwa, Warszawa 1981.

11. Hagele N., Dignath F., Vertical dynamics of the maglev vehicle transrapid. *Multibody System Dynamics*, 2009, 21(3). <https://doi.org/10.1007/s11044-008-9136-0>
12. Han H. S., Yim B. H., Leec N. J.Hur., Y. C. and Kim S. S., "Effect of the guideway's vibrational characteristics on the dynamics of a Maglev vehicle," *Vehicle System Dynamics*, vol. 47, no. 3, pp. 309-324, 2009. <https://doi.org/10.1080/00423110802054342>
13. Han S. H., Kim Y. J., Shin B. C., Kim B. H., Simulation of dynamic interaction between Maglev and guideway using FEM. *Maglev 2006*, Dresden, 2006.
14. Hayashikawa T., Watanabe N., Dynamic behavior of continuous beams with moving loads *J Eng Mech Divis, ASCE*, 107 (1981), pp. 229-246 <https://doi.org/10.1061/JMCEA3.0002694>
15. Hu J., Ma W., Chen X. and Luo S., "Levitation Stability and Hopf Bifurcation of EMS Maglev Trains," *Mathematical Problems in Engineering*, 2020. <https://doi.org/10.1155/2020/2936838>
16. Kim K. J., Han J. B., Han H. S., and Yang S. J., Coupled vibration analysis of maglev vehicle-guideway while standing still or moving at low speeds, *Vehicle System Dynamics*, vol. 53, no. 4, pp. 587–601, 2015. <https://doi.org/10.1080/00423114.2015.1013039>
17. Kim, T.K.; Kim, K.H.; Kwon, H.B., Aerodynamic characteristics of a tube train, *J. Wind Eng. Ind. Aerodyn.* 2011, 99, 1187–1196. <https://doi.org/10.1016/j.jweia.2011.09.001>
18. Kisilowski J., Kowalik R. Displacements of the Levitation Systems in the Vehicle Hyperloop. *Energies*. 2020; 13(24):6595. <https://doi.org/10.3390/en13246595>
19. Kisilowski J., *Dynamika Układu Mechanicznego Pojazd Szynowy—Tor*, PWN, Warszawa, Poland, 1991.
20. Kong E., Song J. S., Kang B. B. and Na S., Dynamic response and robust control of coupled maglev vehicle and guideway system. *Journal of Sound and Vibration*, 2011, vol. 330, no. 25, pp. 6237–6253. <https://doi.org/10.1016/j.jsv.2011.05.031>
21. Kowalik R., Kisilowski J., Numerical Testing of Switch Point Dynamics—A Curved Beam with a Variable Cross-Section. *Materials* 2020, 13(3), 701. <https://doi.org/10.3390/ma13030701>
22. Kowalik R., Kisilowski J., The Vision System for Diagnostics of Railway Turnout Elements. *Management Perspective for Transport Telematics*, Springer, 2018, Volume 897 https://doi.org/10.1007/978-3-319-97955-7_15
23. Lee, J.-S., Kwon, S.-D., Kim, M.-Y., & Yeo, I. H., A parametric study on the dynamics of urban transit maglev vehicle running on flexible guideway bridges. *Journal of Sound and Vibration*, 328(3), 301–317, (2009). doi:10.1016/j.jsv.2009.08.010
24. Li J. H., Li J. and Zhou D. F., "Self-excited vibration problems of Maglev vehicle-bridge interaction system," *J. Cent. South Univ.*, vol. 21, no. 11, pp. 4184-4192, 2014. <https://doi.org/10.1007/s11771-014-2414-5>
25. Li X., Wang D., Liu D., Xin L. and Zhang X., "Dynamic analysis of the interactions between a low-to-medium speed Maglev train and a bridge: field test results of two typical bridges," *Proceedings of the Institution of Mechanical Engineers, Part F: Journal of Rail and Rapid Transit*, vol. 36, pp. 2039-2059, 2018. <https://doi.org/10.1177/0954409718758502>
26. Lingaitis LP, Lebedevas S, Liudvinavičius L. Evaluation of the operational reliability and forecasting of the operating life of the power train of the freight diesel locomotive fleet. *Eksplatacija i Niezawodność – Maintenance and Reliability* 2014; 16 (1): 73–79.
27. Liu Y., Deng W. and Gong P., Dynamics of the Bogie of Maglev Train with Distributed Magnetic Forces, *Shock and Vibration*, Volume 2015,1-15. <https://doi.org/10.1155/2015/896410>
28. Mas Soldevilla J., Dynamic analysis and stability study of the electromagnetic suspension levitation system of the Hyperloop, Hyperloop case, Delft University of Technology, 2022
29. Maximov, S.; Gonzalez-Montañez, F.; Escarela-Perez, R.; Olivares-Galvan, J.C.; Ascencion-Mestiza, H. Analytical Analysis of Magnetic Levitation Systems with Harmonic Voltage Input, *Actuators* 2020, 9, 82. <https://doi.org/10.3390/act9030082>
30. Musk, E., *Hyperloop Alpha*; SpaceX: Hawthorne, CA, USA, 2013.
31. Nicholas A. A., Mohammad M.K., Exploring Bridge Dynamics for Ultra-high-speed, Hyperloop, Trains, *Structures* Volume 14, June 2018, Pages 69-74 <https://doi.org/10.1016/j.istruc.2018.02.006>
32. Oh J. S., Kang T., Ham S., Lee K. S., Jang Y. J., Ryou H. S., Ryu J., Numerical Analysis of Aerodynamic Characteristics of Hyperloop System. *Energies*. 2019, 12. <https://doi.org/10.3390/en12030518>
33. Opgenoord, M.M.; Caplan, P., On the Aerodynamic Design of the Hyperloop Concept, In *Proceedings of the 35th AIAA Applied*

- Aerodynamics Conference, Denver, CO, USA, 5–9 June 2017, p. 3740. <https://doi.org/10.2514/1.J057103>
34. Post R. F., Ryutov D. D., The Inductrack approach to magnetic levitation. *IEEE Trans. Appl. Supercond.* 2000, 10, 901–904. doi: 10.1109/77.828377
 35. Przystupa K., Qin Z., Zabolotnii S., Pohrebennyk V., Mogilei S., Zhongju C., Gil L., Constructing Reference Plans of Two-Criteria Multimodal Transport Problem, *Transport and Telecommunication*, vol. 22, no. 2, pp. 129-140, 2021. <https://doi.org/10.2478/ttj-2021-0010>
 36. Rymarczyk T., Kozłowski E., Kłosowski G., Electrical impedance tomography in 3D flood embankment testing – elastic net approach, *Transactions of the Institute of Measurements and Control*, vol. 42, no. 2, pp. 680-690, 2020. <https://doi.org/10.1177/0142331219857374>
 37. Rymarczyk T., Kozłowski E., Tchórzewski P., Kłosowski G., Adamkiewicz P., Applying the logistic regression in electrical impedance tomography to analyze conductivity of the examined objects, *International Journal of Applied Electromagnetics and Mechanics*, vol. 64, no. S1, pp. S235-S252, 2020. DOI: 10.3233/JAE-209520
 38. Sadeghi S., Saeedifard M. and Bobko C., "Dynamic Modeling and Simulation of Propulsion and Levitation Systems for Hyperloop," 2021 13th International Symposium on Linear Drives for Industry Applications (LDIA), Wuhan, China, 2021, pp. 1-5, doi: 10.1109/LDIA49489.2021.9505882.
 39. Sawczuk W, Merkisz-Guranowska A, Rilo Cañas A-M, Kołodziejcki S. New approach to brake pad wear modelling based on test stand friction-mechanical investigations. *Eksploatacja i Niezawodność – Maintenance and Reliability* 2022; 24 (3): 419–426, <http://doi.org/10.17531/ein.2022.3.3>.
 40. Shi X. H, She L. H. and Chang W. S., "The bifurcation analysis of the EMS maglev vehicle-coupled-guideway system," *Acta Mechanica Sinica*, vol. 36, pp. 634-640, 2004. doi: 10.6052/0459-1879-2004-5-2003-357
 41. Świdorski A., Borucka A., Grzelak M., Gil L., Evaluation of Machinery Readiness using Semi-Markov Processes, *Applied Sciences*, vol. 10, no. 4, 1541, 2020. <https://doi.org/10.3390/app10041541>
 42. Talikdar R. P. and Talukdar S., "Dynamic Analysis of High-Speed MAGLEV Vehicle-Guideway," *Urban Rail Transport*, vol. 2, no. 2, pp. 71-84, 2016. <https://doi.org/10.1007/s40864-016-0039-8>
 43. Taylor, C.; Hyde, B.; Barr, L., *Hyperloop Commercial Feasibility Analysis: High Level Overview*, Cleveland, 2016. https://rosap.nhtl.gov/view/dot/12308/dot_12308_DS1.pdf
 44. Xu J., Chen C., Gao D., Luo S. and Qian Q., "Nonlinear dynamic analysis on Maglev train system with flexible guideway and double time-delay feedback control," *Journal of Vibroengineering*, vol. 19, no. 8, pp. 6346-6362, 2017. <https://doi.org/10.21595/jve.2017.18970>
 45. Yan B., Dai G.L., Hu N., Recent development of design and construction of short span high-speed railway bridges in China *Eng Struct*, 100 (2015), pp. 707-717, 10.1016/j.engstruct.2015.06.050
 46. Yang, Y.; Wang, H.; Benedict, M.; Coleman, D., Aerodynamic simulation of high-speed capsule in the Hyperloop system, In *Proceedings of the 35th AIAA Applied Aerodynamics Conference*, Denver, CO, USA, 5–9 June 2017; p. 3741. <https://doi.org/10.2514/6.2017-3741>
 47. Yau J. D., "Vibration Control of Maglev vehicles travelling over a flexible guideway," *Journal of Sound and Vibration*, vol. 321, pp. 184-200, 2009. <https://doi.org/10.1016/j.jsv.2008.09.030>
 48. Zhang M., Luo S. and Gao C., "Research on the mechanism of a newly developed levitation frame with mid-set air spring," *Vehicle System Dynamics*, vol. 56, no. 12, pp. 1797-1816, 2018. <https://doi.org/10.1080/00423114.2018.1435892>
 49. Zhang, Y., Numerical simulation and analysis of aerodynamic drag on a subsonic train in evacuated tube transportation, *J. Modern Transp.* 2012, 20, 44–48. <https://doi.org/10.1007/BF03325776>
 50. Zhao C. F. and Zhai W. M., Maglev vehicle/guideway vertical random response and ride quality, *Vehicle System Dynamics*, vol. 38, no. 3, pp. 185–210, 2002.
 51. Zheng X. J., Wu J. J., Zhou Y. H., Numerical analysis on dynamic control of five-degree-of-freedom maglev vehicle moving on flexible guideways, *Journal of Sound and Vibration*, 235 (1), (2000). <https://doi.org/10.1006/jsvi.1999.2911>
 52. Zhou D. F., Hansen C. H., and Li J., Application of least mean square algorithm to suppression of Maglev track-induced self excited vibration. *Journal of Sound and Vibration*, 2011, vol. 330, no. 24, pp. 5791–5811 <https://doi.org/10.1016/j.jsv.2011.07.021>